Chlamydomonas reinhardtii formin FOR1 and profilin PRF1 are optimized for acute rapid actin filament assembly

Jenna R. Christensen[a,†], Evan W. Craig[b,†], Michael J. Glista[a], David M. Mueller[b], Yujie Li[a], Jennifer A. Sees[a], Shengping Huang[c], Cristian Suarez[a], Laurens J. Mets[a,*], David R. Kovar[a,d,*], and Prachee Avasthi[b,c,*]

[a]Department of Molecular Genetics and Cell Biology and [d]Department of Biochemistry and Molecular Biology, The University of Chicago, Chicago, IL 60637; [b]Department of Anatomy and Cell Biology and [c]Department of Ophthalmology, University of Kansas Medical Center, Kansas City, KS 66103

ABSTRACT **The regulated assembly of multiple filamentous actin (F-actin) networks from an actin monomer pool is important for a variety of cellular processes. *Chlamydomonas reinhardtii* is a unicellular green alga expressing a conventional and divergent actin that is an emerging system for investigating the complex regulation of actin polymerization. One actin network that contains exclusively conventional F-actin in *Chlamydomonas* is the fertilization tubule, a mating structure at the apical cell surface in gametes. In addition to two actin genes, *Chlamydomonas* expresses a profilin (PRF1) and four formin genes (FOR1–4), one of which (FOR1) we have characterized for the first time. We found that unlike typical profilins, PRF1 prevents unwanted actin assembly by strongly inhibiting both F-actin nucleation and barbed-end elongation at equimolar concentrations to actin. However, FOR1 stimulates the assembly of rapidly elongating actin filaments from PRF1-bound actin. Furthermore, *for1* and *prf1-1* mutants, as well as the small molecule formin inhibitor SMIFH2, prevent fertilization tubule formation in gametes, suggesting that polymerization of F-actin for fertilization tubule formation is a primary function of FOR1. Together, these findings indicate that FOR1 and PRF1 cooperate to selectively and rapidly assemble F-actin at the right time and place.**

Monitoring Editor
Laurent Blanchoin
CEA Grenoble

Received: Aug 20, 2019
Revised: Oct 10, 2019
Accepted: Oct 24, 2019

INTRODUCTION

The actin cytoskeleton is a dynamic system important for diverse cellular processes. *Chlamydomonas reinhardtii* expresses a single conventional actin, IDA5, with 90% identity to mammalian actin, as well as an unconventional actin, NAP1 (Lee *et al.*, 1997; Kato-Minoura *et al.*, 1998), with low identity to mammalian actin (64%). *ida5* mutants have limited phenotypic consequences (Kato-Minoura *et al.*, 1997), likely because NAP1 is up-regulated on IDA5 perturbation (Hirono *et al.*, 2003; Onishi *et al.*, 2018) and has compensatory functions (Jack *et al.*, 2019). The presence of a perinuclear filamentous actin (F-actin) network has been recently established by both a fluorescent Lifeact peptide (Avasthi *et al.*, 2014; Onishi *et al.*, 2016) and an optimized phalloidin labeling protocol (Craig and Avasthi, 2019; Craig *et al.*, 2019). Additionally, a population of F-actin also localizes at the base of the flagella, where it is important for flagellar assembly and proper intraflagellar transport (Avasthi *et al.*, 2014; Jack *et al.*, 2019). Previously, cytokinesis was not shown to require an

This article was published online ahead of print in MBoC in Press (http://www.molbiolcell.org/cgi/doi/10.1091/mbc.E19-08-0463) on October 30, 2019.

The authors declare no competing interests.

†Equal contribution.

Author contributions: conceptualization: J.R.C., M.J.G., L.J.M., P.A., and D.R.K.; methodology: J.R.C., M.J.G., L.J.M., D.R.K., and P.A.; data collection and analysis: J.R.C., M.J.G., E.W.C., D.M.M., Y.L., J.A.S., S.H., and C.S.; writing–original draft preparation: J.R.C., M.G., and P.A.; writing–reviewing and editing: J.R.C., E.W.C., D.M.M., P.A., and D.R.K.; funding acquisition: J.R.C., D.R.K., and P.A.; resources: L.J.M., D.R.K., and P.A.; supervision: D.R.K. and P.A.

*Address correspondence to: Prachee Avasthi (pavasthi@kumc.edu); David R. Kovar (drkovar@uchicago.edu); Laurens J. Mets (mets@uchicago.edu).

Abbreviations used: DMSO, dimethylsulfoxide; F-actin, filamentous actin; FOR1, *Chlamydomonas reinhardtii* formin 1; G-actin, globular actin; LatB, latrunculin B; PRF1, *Chlamydomonas reinhardtii* profilin; PRR, proline-rich repeat; RT, reverse transcription; sub, subunit; TIRF, total internal reflection fluorescence.

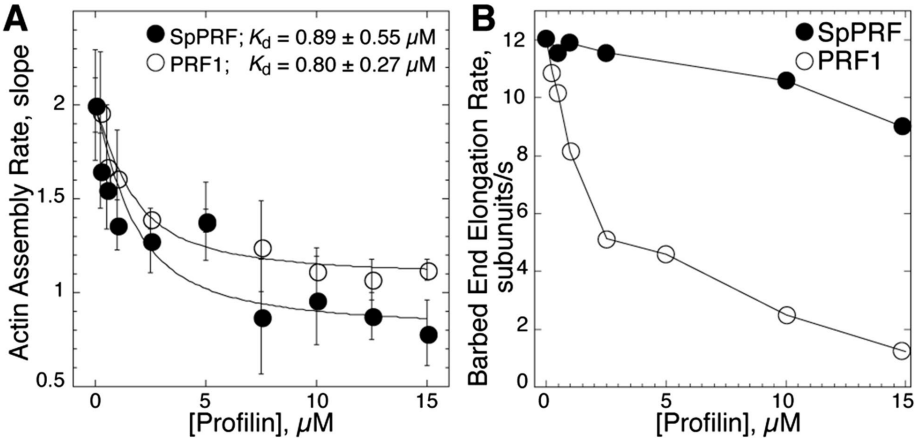

FIGURE 1: PRF1 inhibits nucleation and elongation of actin filaments. (A) Slopes of spontaneous pyrene actin assembly assays (1.5 μM Mg-ATP actin, 20% pyrene labeled) with increasing concentrations of fission yeast profilin SpPRF or *C. reinhardtii* profilin PRF1. Curve fits reveal affinities of SpPRF and PRF1 for actin monomer. Error bars = SEM. Values reported are mean ± SEM for $n = 3$ independent trials. (B) Barbed-end elongation rates of 1.5 μM Mg-ATP actin (10% Alexa-488 labeled) in the presence of increasing concentrations of SpPRF or PRF1, measured by TIRF microscopy.

F-actin network, as proliferation is latrunculin B (LatB) and cytochalasin D insensitive and *ida5* null mutants produce normal cleavage furrows (Harper *et al.*, 1992; Kato-Minoura *et al.*, 1997; Onishi *et al.*, 2016). This finding left open the possibility that cytokinesis might instead utilize LatB-insensitive NAP1, which is up-regulated during LatB treatment (Onishi *et al.*, 2016, 2018). Acute disruption of both IDA5 and NAP1 in *Chlamydomonas* using a combination of mutants and inhibitors results in slightly less efficient cleavage furrow formation and division that may be caused by delays in chloroplast division (Onishi *et al.*, 2019). However, division proceeds, so a different mechanism of cytokinesis primarily involving microtubules may be used in these cells (Onishi *et al.*, 2019).

Another clearly defined F-actin network in *Chlamydomonas* is the fertilization tubule. The fertilization tubule is an F-actin–rich structure found in mating type plus gametes (Detmers *et al.*, 1983, 1985), which during mating protrudes from the "doublet zone", a region between the two flagella (Detmers *et al.*, 1983). Phallacidin staining of F-actin strongly labels fertilization tubules (Detmers *et al.*, 1985), and isolation of fertilization tubules has revealed actin as a major component (Wilson *et al.*, 1997). Additionally, null mutants lacking conventional actin cannot form fertilization tubules (Kato-Minoura *et al.*, 1997). The context-dependent formation of this well-defined F-actin structure in *Chlamydomonas* provides an exceptional opportunity to understand how a cell is capable of precisely regulating its actin cytoskeleton so that actin polymerization occurs only at a very specific place and time.

Chlamydomonas expresses a profilin (PRF1) that, like other profilins, inhibits the nucleation of actin monomers, preventing unwanted actin assembly (Kovar *et al.*, 2001). We have identified a *Chlamydomonas* formin (FOR1) actin assembly factor, which has not been characterized and its cellular role in *Chlamydomonas* not yet determined. Therefore, we sought to characterize the formin FOR1 and determine how FOR1 assembles actin monomers bound to PRF1. Additionally, we wished to determine the role of FOR1 in *Chlamydomonas* cells. We found that in addition to inhibiting nucleation, PRF1 potently inhibits the barbed-end elongation of actin filaments at relatively low concentrations. However, FOR1 overcomes this inhibition and swiftly assembles PRF1-bound actin monomers into actin filaments that elongate rapidly. *Chlamydomonas* cells treated with the formin inhibitor SMIFH2 do not form fertilization tubules, nor do *for1* or *prf1-1* mutants, suggesting that the collective activities of PRF1 and FOR1 regulate acute F-actin assembly for mating in *Chlamydomonas*.

RESULTS

PRF1 inhibits nucleation and elongation of actin filaments

Plant, fungal, and metazoan cells maintain a large pool of unassembled globular actin (G-actin) bound to profilin (Carlsson *et al.*, 1977; Kaiser *et al.*, 1999; Lu and Pollard, 2001). Profilin inhibits the unwanted nucleation of new actin filaments (Pollard and Cooper, 1984). Once an actin filament has been formed, profilin-bound actin monomers are added to the barbed end of growing actin filaments to varying degrees depending on the type of actin. In experiments using muscle actin, profilin-bound actin adds to the barbed end to the same degree as free monomers (Pollard and Cooper, 1984). However, in other studies using muscle actin, β-actin, or nonmuscle actin, profilin-bound actin slows the barbed-end elongation rate (Gutsche-Perelroizen *et al.*, 1999; Kinosian *et al.*, 2002; Hansen and Mullins, 2010). Additionally, mammalian profilins promote nucleotide exchange (such as ADP to ATP) of actin, although plant profilins do not (Mockrin and Korn, 1980; Goldschmidt-Clermont *et al.*, 1991; Perelroizen *et al.*, 1994, 1996).

Chlamydomonas profilin PRF1 is found throughout the cytoplasm and flagellar compartments of the cell, but is enriched at the base of the flagella in vegetative cells and below the fertilization tubule in mating type plus gametes (Kovar *et al.*, 2001). Unlike typical profilins, *Chlamydomonas* PRF1 inhibits the nucleotide exchange of bound G-actin (Kovar *et al.*, 2001). PRF1 might therefore inhibit actin assembly in cells more potently than other profilins. We performed a series of biochemical experiments to determine how PRF1 affects actin assembly. As we do not have purified *Chlamydomonas* actin, we used skeletal muscle actin for all actin biochemistry experiments. We confirmed that the spontaneous assembly of actin monomers was inhibited by PRF1 in a concentration-dependent manner (Figure 1A), like other profilins including fission yeast SpPRF (K_d = 0.89 ± 0.55 μM), revealing a relatively high-affinity for actin monomers (K_d = 0.80 ± 0.27 μM). Surprisingly, by directly observing the spontaneous assembly of 1.5 μM Mg-ATP actin monomers using total internal reflection fluorescence (TIRF) microscopy, we found that unlike other profilins such as SpPRF, PRF1 also significantly inhibits the barbed-end elongation of actin filaments at concentrations where the ratio of PRF1 to actin is equal or only two- to threefold higher (Figure 1B). Therefore, PRF1 is a multifaceted inhibitor of actin polymerization that potently prevents both actin filament nucleation and elongation.

An inhibitory profilin such as PRF1 is ideal to prevent unwanted spontaneous actin assembly. However, as F-actin is present within the fertilization tubule during mating, F-actin polymerization must occur at the correct time and place. Therefore, we speculated that an actin assembly factor such as a formin could be responsible for

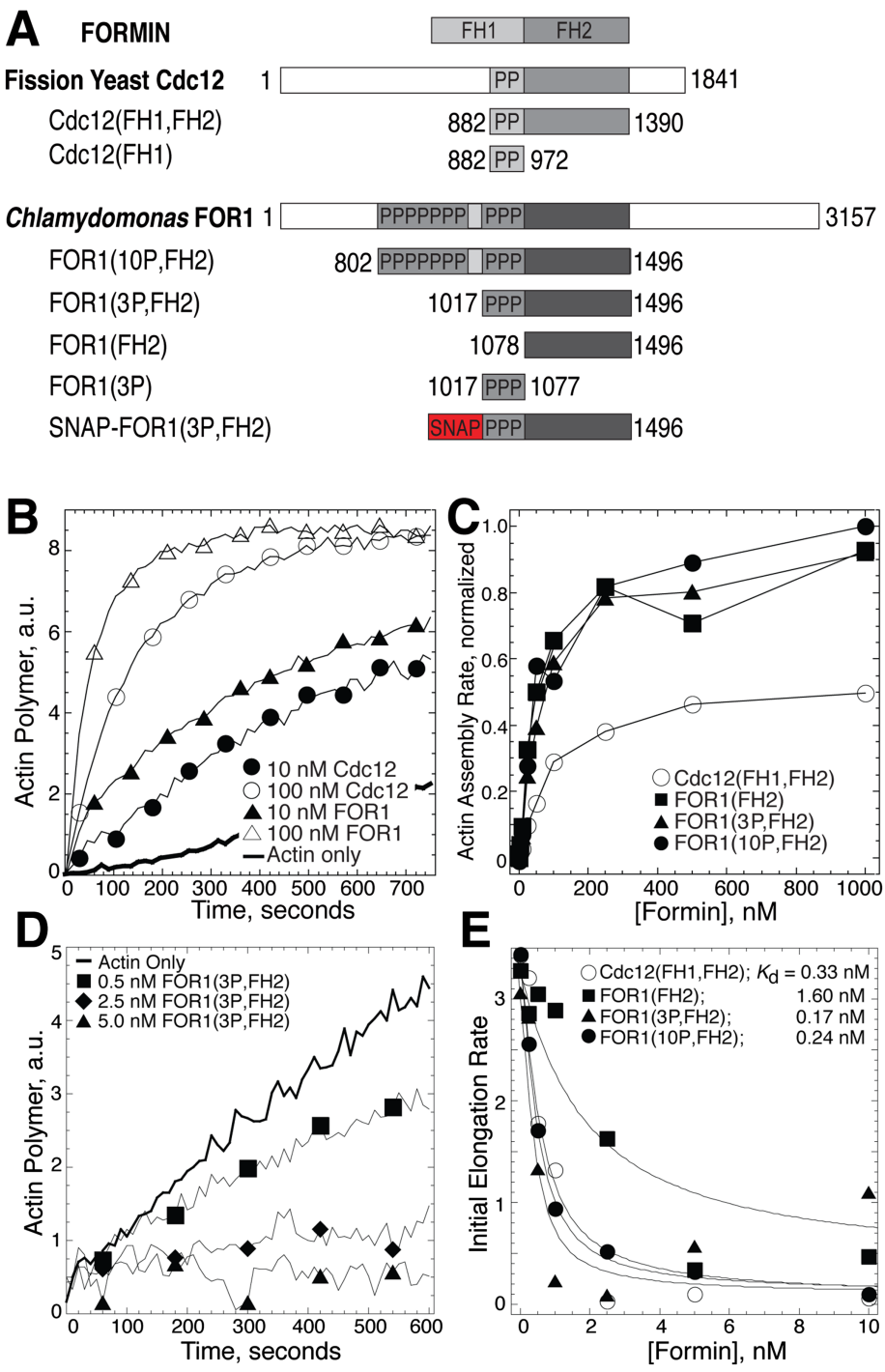

FIGURE 2: FOR1 efficiently nucleates actin filaments that elongate slowly. (A) Domain organizations and constructs used in this study of fission yeast formin Cdc12 and *C. reinhardtii* formin FOR1. Numbers denote amino acid residues. Each "P" indicates a putative profilin binding site of at least six prolines within eight residues. (B, C) Spontaneous assembly of 2.5 μM Mg-ATP actin monomers (20% pyrene labeled). (B) Pyrene fluorescence over time for actin alone (thick curve) and with 10 (●) or 100 (○) nM Cdc12(FH1,FH2) or 10 (▲) and 100 (△) nM FOR1(3P,FH2). (C) Dependence of the normalized actin assembly rate (slope) on the concentration of Cdc12(FH1,FH2) (○), FOR1(FH2) (■), FOR1(3P,FH2) (▲), and FOR1(10P,FH2) (●). (D, E) Seeded assembly of 0.2 μM Mg-ATP actin monomers (20% pyrene labeled) onto 0.5 μM preassembled filaments. (D) Pyrene fluorescence over time for actin alone (thick line) or in the presence of 0.5 (□), 1.0 (◆), or 2.5 (▲) nM FOR1(3P,FH2). (E) Dependence of the initial barbed-end assembly rate on formin concentration. Curve fits revealed equilibrium dissociation constants of 0.33 nM for Cdc12(FH1,FH2) (○), 1.6 nM for FOR1(FH2) (■), 0.17 nM for FOR1(3P,FH2) (▲), and 0.24 nM for FOR1(10P,FH2) (●).

rapid actin assembly at fertilization tubule sites.

Formin identification in *C. reinhardtii*

A BLAST search for conserved formin FH2 domain lasso and post sequences using mouse formin (CAA37668—amino acids 986–1251) as query identified a *Chlamydomonas* gene locus (Cre03.g166700 in the version 5.6 genome assembly) as a candidate formin. Manual inspection of the genome region upstream of the lasso element revealed an FH1 domain containing at least three proline-rich repeats (PRRs) in the same reading frame with typical 6–8–amino acid spacing between. An additional seven PRRs with typical short (8–12 amino acids) spacing were found further upstream of an unusually long spacer of 37 amino acids. A Kazusa DNA Research Institute EST sequence from *Chlamydomonas* (HCL081g04) confirmed splicing of the putative FH2 domain to the first three PRRs of the FH1 domain. A full-length cDNA sequence provided by Susan Dutcher (personal communication) confirmed expression of the long spacer and all 10 PRR regions within a 3157–amino acid protein (Figure 2A). This formin was named *C. reinhardtii* formin 1 (FOR1). We created bacterial expression constructs containing either three or 10 PRRs along with the FH2 domain and confirmed their ability to stimulate actin polymerization (Figure 2; see below), suggesting that the expressed protein is a formin. There are three other FH2 domain containing genes in *Chlamydomonas*, which we have denoted FOR2 (Cre05.g232900), FOR3 (Cre06.g311250), and FOR4 (Cre04.g229163).

FOR1 efficiently nucleates but weakly elongates actin filaments

Formins are a conserved family of actin assembly factors that nucleate actin filaments. Additionally, formins increase the F-actin elongation rate in the presence of profilin by remaining processively associated with the barbed end (Breitsprecher and Goode, 2013). Formins contain actin assembly FH1 and FH2 domains, which are typically flanked by regulatory regions. Functional formins are dimers, with two FH2 domains interacting head-to-tail to create a donut-shaped dimer capable of creating a stable actin "nucleus" (Otomo *et al.*, 2005) and remaining processively associated with the elongating barbed end of an actin filament (Kovar, 2006). The unstructured FH1 domains are rich in PRRs that bind to profilin and promote rapid association of profilin-actin with the barbed end of an elongating filament. To investigate the actin assembly

properties of the formin FOR1, we created a set of constructs containing the FOR1 FH1 and FH2 domains, alone or in combination (Figure 2A). Because our initial inspection of the FOR1 gene suggested that depending on splicing it contained either three or 10 PRRs within its FH1 domain, we created constructs containing either three or 10 PRRs (FOR1[3P,FH2] or FOR1[10P,FH2], respectively). We focused on constructs containing solely the FH1 and FH2 domains as full-length formins are difficult to purify, and active formin constructs containing only the FH1 and FH2 domains have been extensively studied for numerous formins (Breitsprecher and Goode, 2013). However, as the C-terminal domains of certain formins have been shown to affect their actin assembly properties (Gould *et al.*, 2011), it will be interesting in the future to investigate how additional domains may modify the actin assembly activity of the FH1 and FH2 domains of FOR1.

FOR1's capacity to stimulate actin assembly in the absence of profilin was initially investigated by measuring the effect of FOR1 on actin polymerization over time using spontaneous pyrene actin assembly assays. FOR1 containing the FH2 domain alone (FOR1[FH2]) or both the FH1 and FH2 domains (FOR1[3P,FH2] or FOR1[10P,FH2]) stimulate actin assembly in a nearly identical, concentration-dependent manner (Figure 2, B and C) and more potently than a well-characterized control formin fission yeast Cdc12(FH1,FH2) (Figure 2, B and C) (Kovar *et al.*, 2003; Scott *et al.*, 2011). Though these results reveal that FOR1 increases the overall rate of actin polymerization, spontaneous pyrene actin assembly assays are unable to differentiate between an increase in the nucleation and/or elongation of actin filaments.

To differentiate between the contributions of nucleation and elongation to the overall enhanced polymerization rate, we initially examined the effect of FOR1 on actin filament elongation using seeded pyrene actin assembly assays. In the presence of actin filament seeds, elongation of the seeds dominates the reaction and the contribution of nucleation to the overall actin polymerization rate is eliminated. Addition of FOR1(FH2), FOR1(3P,FH2), or FOR1(10P,FH2) to seeded assembly reactions each reduced the actin assembly rate in a concentration dependent matter (Figure 2, D and E). This result suggests that FOR1 inhibits actin filament elongation, and that the increased actin assembly rate observed in spontaneous pyrene actin assays is due to FOR1-mediated nucleation. Fits of the initial seeded polymerization rates over a range of formin concentrations revealed dissociation rate constants (K_d) for actin filament barbed ends in the low nanomolar range: FOR1(FH2) (K_d = 1.6 nM), FOR1(3P,FH2) (K_d = 0.17 nM), FOR1(10P,FH2) (K_d = 0.24 nM), and Cdc12(FH1,FH2) (K_d = 0.33 nM) (Figure 2E).

Fission yeast profilin SpPRF enhances FOR1-mediated actin assembly

In the absence of profilin, *Chlamydomonas* formin FOR1 has potent nucleation activity but also significantly inhibits actin filament barbed-end elongation, similar to the fission yeast formin Cdc12. However, like other formins (Kovar *et al.*, 2006), Cdc12-associated filaments elongate their barbed ends ~30-fold faster when fission yeast profilin SpPRF is included in the reaction (Kovar *et al.*, 2003; Scott *et al.*, 2011). We hypothesized that profilin would also increase the elongation rate of filaments nucleated by FOR1. We first tested the ability of profilins PRF1 and SpPRF to bind to the FH1 domains of FOR1 and Cdc12. Interestingly, although PRF1 binds much more weakly than SpPRF to nonphysiological poly-L-proline (Figure 3, A and C) (Kovar *et al.*, 2001), PRF1 and SpPRF have similar affinities for the FH1 domains of both FOR1 and Cdc12 (Figure 3, B and C), all with dissociation rate constants (K_d) within the low micromolar range.

We found that PRF1 binds well to the FOR1 FH1 domain. In these binding experiments, the FOR1 FH1 domain is in excess. As a result, the low K_d is likely the result of binding to the single highest affinity binding site within the multiple binding sites within the FH1 domain. However, formin-mediated assembly of profilin-actin requires a variety of interactions, including complementary interactions with profilin and both the FH1 and FH2 domains of the formin (Neidt *et al.*, 2009; Bestul *et al.*, 2015). Therefore, we tested the ability of the FH1 and FH2 domains of FOR1 to assemble profilin-actin. We initially tested the ability of FOR1 to assemble SpPRF-actin, as SpPRF is widely compatible with different formin isoforms (Neidt *et al.*, 2009; Bestul *et al.*, 2015). Spontaneous pyrene actin assembly assays revealed that FOR1 constructs containing both the FH1 and FH2 domains (FOR1[3P,FH2] and FOR1[10P,FH2]) rapidly accelerate actin assembly in the presence of SpPRF (Figure 3, D and E). Conversely, SpPRF inhibits actin assembly by FOR1(FH2), the construct lacking the FH1 domain (Figure 3, D and E). The pyrene actin assembly rates measured for FOR1(3P,FH2) and FOR1(10P,FH2) are significantly greater than those of Cdc12(FH1,FH2) over a range of SpPRF concentrations (Figure 3E), suggesting that SpPRF dramatically increases the barbed-end elongation rate of FOR1-nucleated actin filaments.

PRF1-actin is utilized specifically by FOR1

We next examined the ability of FOR1 to assemble actin monomers bound to PRF1. In spontaneous pyrene actin assembly assays, the pyrene fluorescence measured in reactions containing FOR1 and PRF1 is sharply reduced relative to actin alone or actin in the presence of FOR1 (Figure 3F). This decrease could indicate that PRF1 severely inhibits FOR1-mediated actin assembly as PRF1 severely inhibits actin assembly in the absence of FOR1 (Figure 1). Alternatively, it is possible that PRF1 accelerates FOR1-mediated actin assembly, but the combination of FOR1 and PRF1 specifically excludes assembly of actin labeled on Cys-374 with pyrene, as we have described for other formin and profilin combinations (Kovar *et al.*, 2006; Scott *et al.*, 2011). Therefore, we directly visualized actin filaments formed in spontaneous pyrene actin assembly assays in the presence of different combinations of formin and profilin. After assembling for 600 s, the bulk polymerization reactions were stopped by diluting into TRITC-phalloidin to allow visualization of filaments by fluorescence microscopy (Figure 3G). In the absence of profilin, FOR1 produces many small actin filaments (average length, 2.7 ± 4.0 μm), indicative of efficient nucleation by FOR1, as suggested by spontaneous pyrene actin assembly assays (Figure 2). Additionally, FOR1 facilitates formation of long actin filaments in the presence of both SpPRF (16.6 ± 10.2 μm) and PRF1 (27.4 ± 17.5 μm). Interestingly, although FOR1 elongates actin filaments similarly well in the presence of SpPRF or PRF1, Cdc12 forms longer filaments in the presence of SpPRF (average length, 16.2 ± 4.9 μm) than PRF1 (4.2 ± 4.9 μm) (Figure 3G), suggesting that PRF1 is tailored for elongation by FOR1. Together, these results indicate that FOR1 is capable of efficient actin filament nucleation, and in the presence of its complementary profilin PRF1, rapidly elongates these filaments. In addition, the reduced ability of Cdc12 to elongate PRF1-associated actin suggests that FOR1 and PRF1 are tailored to precisely and rapidly polymerize F-actin.

FOR1 rapidly and processively elongates actin filaments in the presence of PRF1

To directly examine the effect of PRF1 on FOR1-mediated actin assembly, we visualized the assembly of 1 μM Mg-ATP actin (10% Alexa-488 labeled) over time using TIRF microscopy. As we found

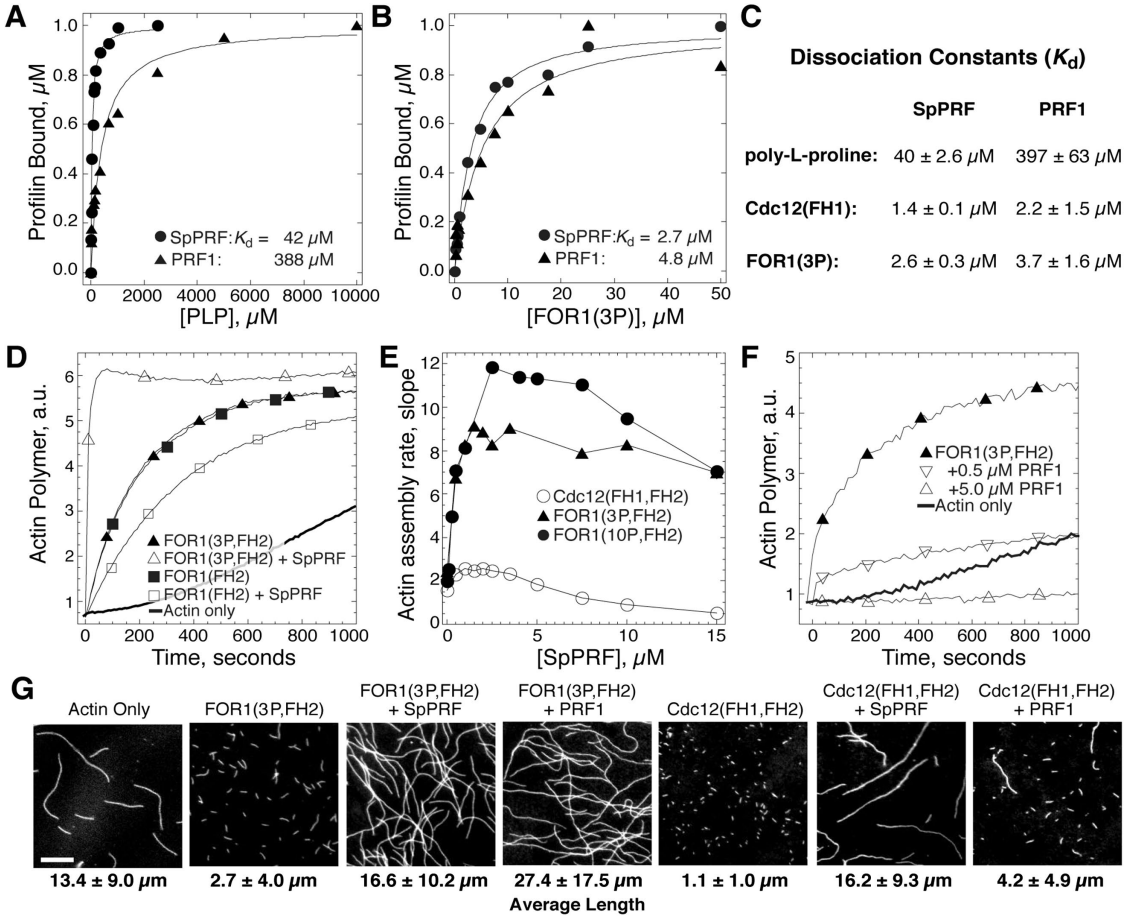

FIGURE 3: FOR1 stimulates the assembly of profilin-actin. (A–C) Affinity of profilin for poly-L-proline and formin FH1 domains. Dependence of fission yeast SpPRF (●) and PRF1 (▲) intrinsic tryptophan fluorescence on the concentration of poly-L-proline (A) and FOR1(3P) (B). (C) Average affinity of SpPRF and PRF1 for poly-L-proline, Cdc12(FH1), and FOR1(3P); $n \geq 3$ experiments. (D–F) Spontaneous assembly of 2.5 μM Mg-ATP actin (20% pyrene labeled). (D) Pyrene fluorescence over time for actin alone (thick curve), with 10 nM FOR1(FH2) in the absence (■) or presence (□) of 2.5 μM SpPRF, and with 10 nM FOR1(3P,FH2) in the absence (▲) or presence (△) of 2.5 μM SpPRF. (E) Dependence of the actin assembly rate (slope) on the concentration of SpPRF for reactions containing 10 nM Cdc12(FH1,FH2) (○), 10 nM FOR1(3P,FH2) (▲), or 10 nM FOR1(10P,FH2) (●). (F) Pyrene fluorescence over time for actin alone (thick curve), and with 10 nM FOR1(3P,FH2) in the absence (▲), or presence (▽) of 0.5 μM or 5.0 μM (△) PRF1. (G) Fluorescence micrographs of actin filaments taken 10 min after the initiation of the indicated reactions with 10 nM formin and 2.5 μM profilin. Samples were labeled with rhodamine-phalloidin and adsorbed to glass coverslips coated with poly-L-lysine. Scale bar, 5 μm.

that FOR1(3P,FH2) assembled F-actin to a similar degree as FOR1(10P,FH2) in several "bulk" actin assembly assays (Figures 2 and 3), we chose to use FOR1(3P,FH2) in the remainder of our biochemistry experiments. Actin filaments alone (control) elongate at a rate of 11.5 subunits (sub)/s (Figure 4A). In the presence of 1 nM FOR1(3P,FH2), two populations of filaments are observed: actin filaments elongating at the control rate (9.1 sub/s, red arrowheads), and actin filaments elongating at a significantly slower rate (0.3 sub/s, blue arrowheads) (Figure 4B). We predict that the slow-growing filaments are bound at their barbed end by FOR1, which significantly reduces their elongation, while filaments elongating at the control rate are not bound by FOR1 (Kovar *et al.*, 2003, 2006). In the presence of 1 nM FOR1 and 2.5 μM PRF1, two distinct populations of filaments are again observed: actin filaments elongating at a rate slower than the control rate (4.2 sub/s) and rapidly elongating actin filaments (63.2 sub/s) (Figure 4C). The assembly rate of internal control filaments is slower in these reactions because PRF1 inhibits actin filament elongation (Figure 1B), while FOR1 can efficiently utilize PRF1-bound actin to rapidly elongate actin filaments. The remarkable 200-fold difference between the elongation rate of FOR1-bound F-actin in the absence (~0.3 sub/s) and presence (~60 sub/s) of PRF1 is one of the largest observed (Kovar, 2006).

Our results suggest that FOR1 remains processively associated with actin filament barbed ends while cooperating with PRF1 to dramatically increase the elongation rate. To directly visualize and confirm this finding, we made a SNAP-tagged construct of FOR1(3P,FH2) that was labeled with SNAP-549 dye for multicolor TIRF microscopy experiments (Figure 5). In the absence of PRF1, SNAP-FOR1(3P,FH2) remains continuously associated with the barbed end of short, slow growing actin filaments (Figure 5A, blue arrowheads), consistent with our finding that FOR1 can nucleate actin filaments but significantly slows actin filament elongation. Conversely, in the presence of PRF1, SNAP-FOR1(3P,FH2)-associated actin filaments elongate rapidly (Figure 5, B and D; Supplemental Movie S1) compared with control filaments (Figure 5C).

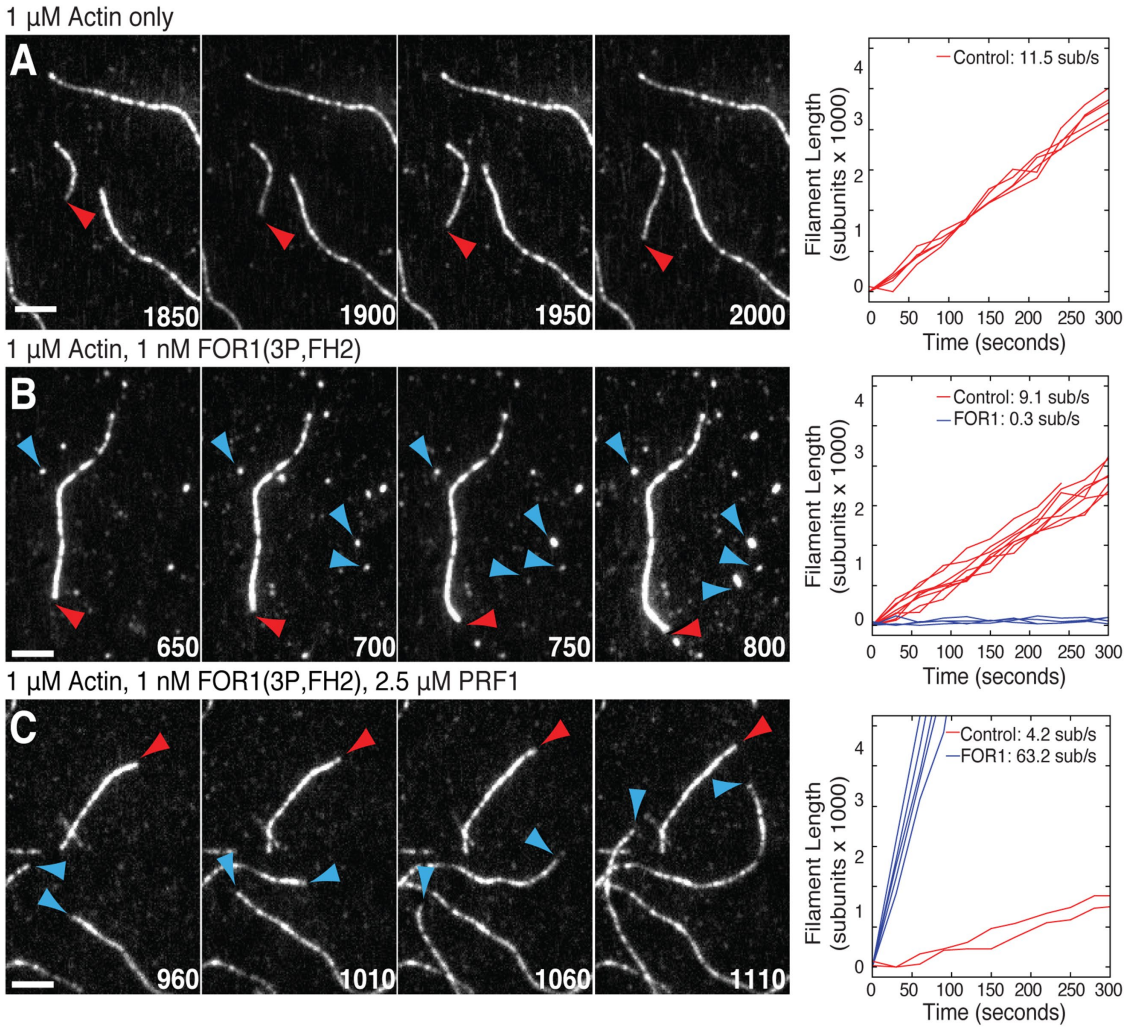

FIGURE 4: FOR1 rapidly elongates actin filaments in the presence of PRF1. (A–C) TIRF microscopy of 1 µM Mg-ATP actin (20% Alexa-488 labeled). Left, Time-lapse micrographs with time in seconds of actin alone (A), with 1 nM FOR1(3P,FH2) (B), or with 1 nM FOR1(3P,FH2) and 2.5 µM PRF1. Red and blue arrowheads denote control (formin independent) and FOR1-dependent filaments, respectively. Scale bars, 5 µm. Right, Rates of filament growth for control (red lines) and FOR1-associated (blue lines) filaments.

Fertilization tubule formation is prevented by the formin inhibitor SMIFH2

PRF1 is a potent inhibitor of actin filament nucleation and elongation. However, PRF1-bound actin can be rapidly assembled by FOR1. We were interested in the role that this tailored protein interaction plays in facilitating actin polymerization in vivo. As the fertilization tubule in *Chlamydomonas* is known to be F-actin rich and appears by EM to contain a parallel array of linear actin filaments (Detmers *et al.*, 1983), we suspected that a formin like FOR1 might assemble the long actin filaments required for fertilization tubule formation in *Chlamydomonas* gametes. To test this, we chemically induced fertilization tubule formation in gametes and stained cells with fluorescent phalloidin to label F-actin (Figure 6, B–H). Fertilization tubules were observed in ~43% of untreated or dimethylsulfoxide (DMSO) (control)-treated induced gametes (Figure 6, B, C, and H). As expected, treatment with 10 µM LatB, which depolymerizes F-actin networks, eliminated fertilization tubules (Figure 6, D and H). We then tested whether chemically inhibiting formins would affect fertilization tubule formation. Formin inhibitor SMIFH2 potently inhibited FOR1-mediated actin assembly in vitro (Figure 6A) (Rizvi *et al.*, 2009). Correspondingly, though 10 µM of formin inhibitor SMIFH2 had little effect on tubule formation (Figure 6, E and H), only 5% of gametes formed fertilization tubules in the presence of 100 µM SMIFH2 (Figure 6, F and H). To address whether fertilization tubule loss with 100 µM SMIFH2 is specific, we also treated cells with 100 µM of Arp2/3 complex inhibitor CK-666 (Nolen *et al.*, 2009). Similar to controls, ~40% of CK-666 cells formed fertilization tubules (Figure 6, G and H), indicating that FOR1-mediated but not Arp2/3 complex-mediated F-actin assembly is required for fertilization tubule formation. Furthermore, we also found that FOR1 is capable of bundling actin filaments to a similar extent as fission yeast formin Fus1, the formin involved in mating projectile formation in fission yeast cells (Supplemental Figure S1), suggesting that in addition to assembling actin filaments, FOR1 could potentially also be involved in bundling actin filaments in the fertilization tubule.

FOR1 and PRF1 mutants fail to form fertilization tubules

SMIFH2 inhibition of fertilization tubule formation suggests that a formin is required to assemble F-actin within the fertilization tubule. However, SMIFH2 is a pan-formin inhibitor that likely has more than one formin target and may have additional nonspecific targets as well (Isogai *et al.*, 2015). As *Chlamydomonas* has four putative

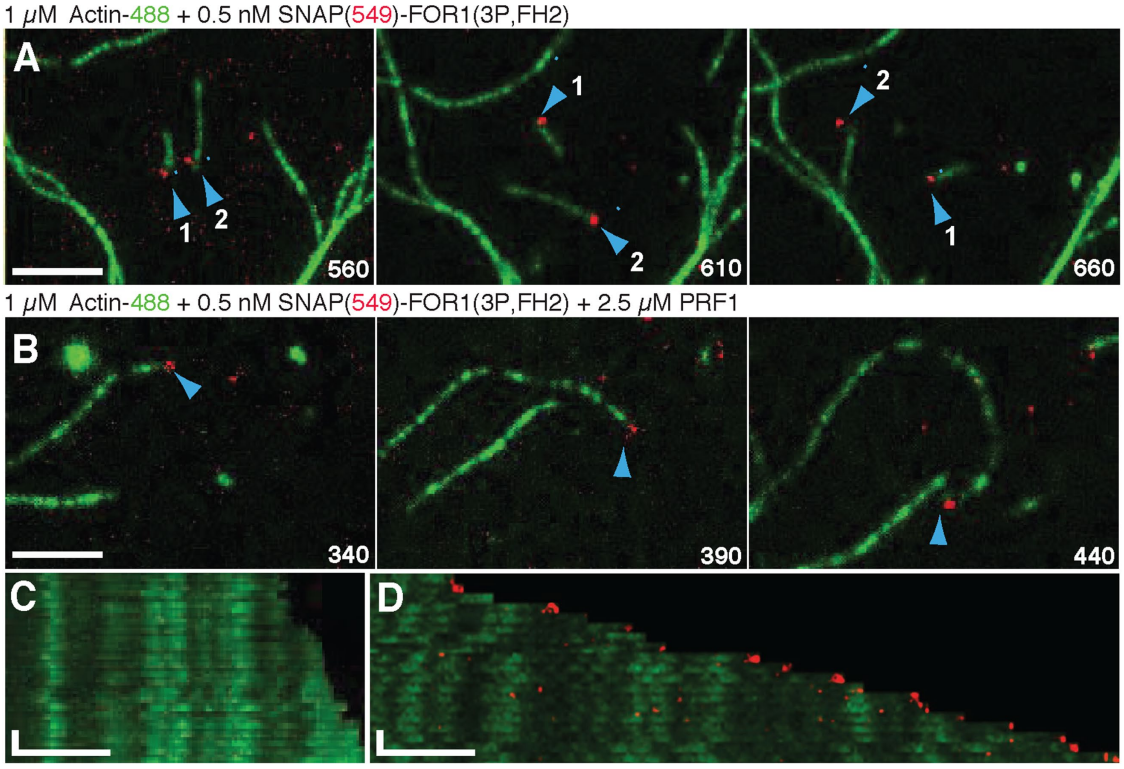

FIGURE 5: FOR1 is processive on F-actin barbed ends in the absence and presence of PRF1. (A–D) Two-color TIRF microscopy of 1 μM Mg-ATP actin (10% Alexa-488 labeled) with 0.5 nM SNAP-FOR1(3P,FH2) (549-labeled) in the presence or absence of 2.5 μM PRF1. Blue arrowheads denote formin-bound filaments. (A) SNAP-FOR1(3P,FH2) (0.5 nM) alone. (B) SNAP-FOR1(3P,FH2) (0.5 nM) in the presence of 2.5 μM PRF1. Scale bars, 5 μm. Time in seconds. (C, D) Kymographs of control (C) and formin-bound (D) filaments from B. Scale bars, *x*-axis, 5 μm. Time bars, *y*-axis, 30 s.

formin genes, we first determined whether FOR1 specifically assembles F-actin for fertilization tubule formation. Several mutants containing insertions in the FOR1 coding sequence were available from the *Chlamydomonas* mutant library (www.chlamylibrary.org). We chose to analyze a mutant with an insertion in exon 3 (Figure 7, A and B), upstream of the FH1 and FH2 domains in FOR1. Disruption of FOR1 was confirmed by the absence of FH2 domain expression (Figure 7C). In activated wild-type gametes, cells form long fertilization tubules between flagella in 89% of cells (N = 200) (Figure 7D). In *for1* insertional mutants, gametes retained their perinuclear actin structures (Figure 7, E, E′, and E″), but began to deform in the region where fertilization tubule extension normally takes place, with no tubule protrusion (Figure 7, E′ and E″, white arrows). Sometimes, a F-actin focus could be seen at the tip of the deformation (Figure 7E′, white arrowhead). These genetic data confirm that FOR1 is required for normal actin filament assembly in fertilization tubules. In the absence of this formin, attempts to form a tubule cause morphological defects at the apical surface of activated gametes. We also tested the ability of mutants of two other formins to make fertilization tubules. *For2* mutants also exhibited a defect in tubule formation but to a reduced extent than *for1* mutants, as some cells could still make tubules (Supplemental Figure S2, A–E). Because these cells did not show a complete loss of tubules, we tested the functional effects of tubule reduction and found reduced rates of cell fusion (Supplemental Figure S2F). In contrast, *for3* mutants showed no differences in tubule formation from the wild type (Supplemental Figure S3). No mutants with an insertion in the coding region of FOR4 were available in the *Chlamydomonas* mutant library. Our data suggest that while FOR2 may also be involved in fertilization tubule formation or maintenance, FOR1 is the primary formin required for proper fertilization tubule formation.

To further characterize the importance of the formin–profilin interaction on fertilization tubule formation in vivo, we tested whether a temperature-sensitive mutant of PRF1 (*prf1-1*) (Tulin and Cross, 2014; Onishi *et al.*, 2018) was capable of forming fertilization tubules. It has been previously demonstrated that little PRF1 is detectable even at the permissive temperature in *prf1-1* mutants (Onishi *et al.*, 2018). Correspondingly, *prf1-1* mutants showed a complete inability to generate fertilization tubules compared with wild-type controls at both the permissive and restrictive temperatures (Figure 8). However, PRF1 is thought to protect monomeric conventional actin IDA5 from degradation in *Chlamydomonas*, as IDA5 protein is lost and NAP1 up-regulated at the permissive temperature in *prf1-1* mutants (Onishi *et al.*, 2018). Given that IDA5 is required for fertilization tubule formation (Kato-Minoura *et al.*, 1997), the *prf1-1* mutant phenotype may also be attributable to the loss of IDA5. We additionally tested whether a mutant of the unconventional actin NAP1 (*nap1*) (Onishi *et al.*, 2016) was capable of forming fertilization tubules. We found that mutants of NAP1 (in which IDA5 expression is abundant) showed no defect in fertilization tubule formation (Supplemental Figure S4). While NAP1 was previously observed within fertilization tubules using NAP1-specific antibodies (Hirono *et al.*, 2003), this population seems inessential for tubule formation.

DISCUSSION

PRF1 as a regulator of F-actin assembly

Unlike typical profilins that primarily inhibit only the nucleation of new actin filaments, PRF1 is an unusual profilin that at relatively low concentrations dramatically prevents actin assembly by inhibiting

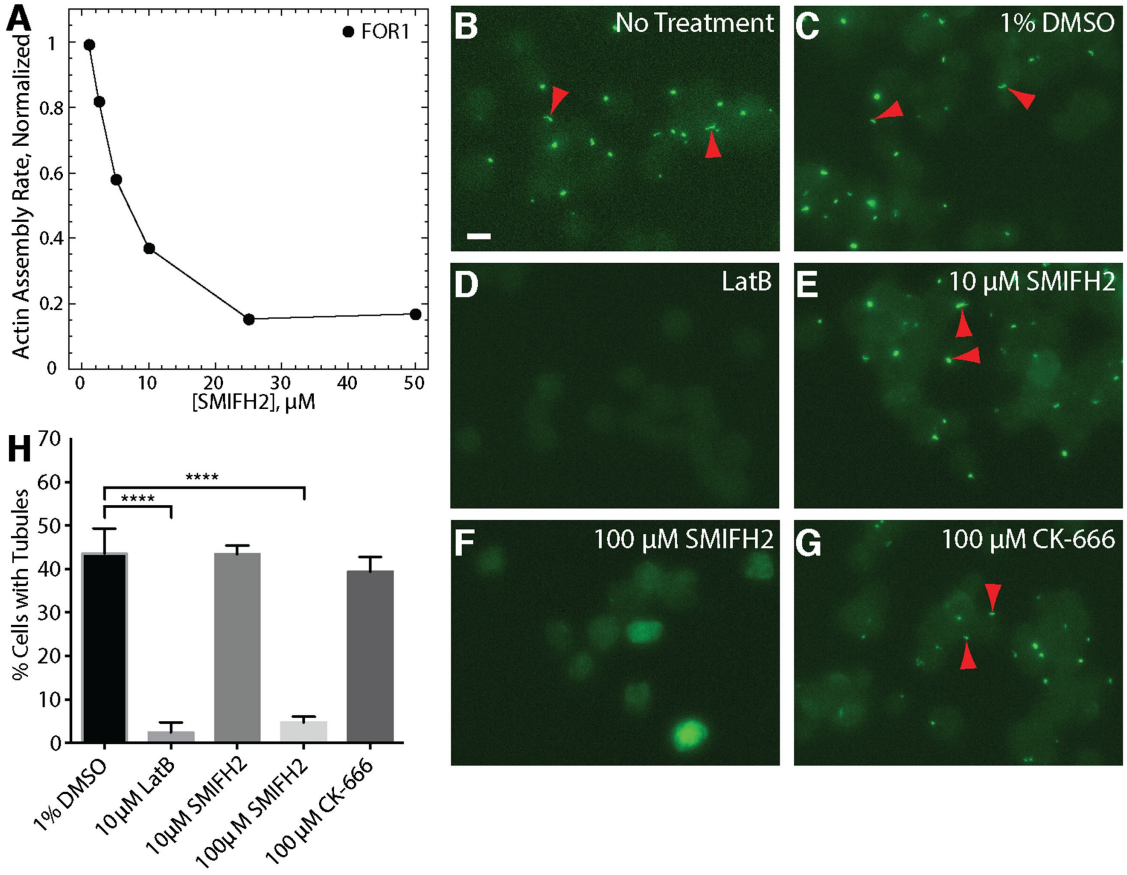

FIGURE 6: SMIFH2 formin inhibition disrupts fertilization tubules in *Chlamydomonas* gametes. (A) Normalized actin assembly rate of FOR1(3P,FH2) (●) in the presence of increasing concentrations of formin inhibitor SMIFH2. (B–F) Representative fluorescent micrographs of *Chlamydomonas* gamete fertilization tubules (red arrowheads) labeled with the F-actin marker 488-phalloidin. Scale bar, 5 μm. (B) Untreated control. (C) DMSO (1%) control. (D) Actin depolymerization of drug LatB (10 μM). (E) Formin inhibitor SMIFH2 (10 μM). (F) SMIFH2 (100 μM). (G) Arp2/3 complex inhibitor CK-666 (100 μM). (H) Quantification of the percentage of cells with fertilization tubules following indicated treatments; $n = 3$ independent experiments. Values reported are mean ± SD, ****$p < 0.0001$.

both the nucleation and barbed-end elongation of actin filaments. This effect on actin filament elongation is potentially due to one of two mechanisms: 1) PRF1-bound actin monomers may be a poor substrate for barbed-end elongation or 2) PRF1 may have an enhanced affinity for the actin filament barbed end. However, our experiments do not discriminate between these two mechanisms. Other profilins have also been shown to decrease barbed-end elongation (Courtemanche and Pollard, 2013; Pernier *et al.*, 2016), though at concentrations that are 5–10 times higher than PRF1 (Figure 1B). As PRF1 inhibits nucleation, elongation, and the ADP-to-ATP exchange of bound actin monomers (Kovar *et al.*, 2001), PRF1 is a tight regulator of the actin monomer pool, inhibiting spontaneous actin filament assembly in the cell.

Though PRF1 prevents spontaneous actin assembly, FOR1 overcomes the inhibitory effect of PRF1 and utilizes PRF1-bound actin to rapidly assemble actin filaments for the fertilization tubules in mating gametes. Because we do not have purified *Chlamydomonas* actin, all of the biochemical experiments to determine how PRF1 affects actin assembly in the absence and presence of FOR1 were performed with muscle actin. Although it is possible that PRF1 and FOR1 will behave quantitatively differently with *Chlamydomonas* actin, our results with muscle actin are very likely to be qualitatively similar given that muscle and conventional IDA5 *Chlamydomonas* actin are 90% identical and 95% similar (*Chlamydomonas* genome v5.5, Phytozome; Merchant *et al.*, 2007). We have previously shown that the particular profilin defines the rate of formin-mediated actin assembly (Neidt *et al.*, 2009). The presence of tailored formin–profilin pairs (Bestul *et al.*, 2015) suggests that this interaction is crucial for controlling utilization of an actin monomer pool. The *Chlamydomonas* profilin PRF1 appears to be an extreme example of this, as PRF1-bound actin does not nucleate or elongate well in the absence of FOR1. The other *Chlamydomonas* formins may nucleate and/or elongate PRF1-bound actin to different extents, promoting proper regulation of the profilin-actin pool toward assembly of specific F-actin networks. The FH2 domain of formin binds within the hydrophobic cleft between actin subdomains 1 and 3 (Otomo *et al.*, 2005). Of the 11 residues that line the hydrophobic cleft, 100% are conserved in IDA5. In NAP1, eight of the residues are conserved and two are similar amino acids (Supplemental Figure S5). Of the 21 actin residues that contact profilin (Schutt *et al.*, 1993), 15 are conserved in NAP1 and an additional three are strongly similar amino acid substitutions. The differences between the unconventional NAP1 and the conventional *Chlamydomonas* actin add another layer to the complex regulation of actin assembly in this organism. Future work will involve deciphering how the formins utilize both the conventional and unconventional actins in *Chlamydomonas* to promote specific cellular processes.

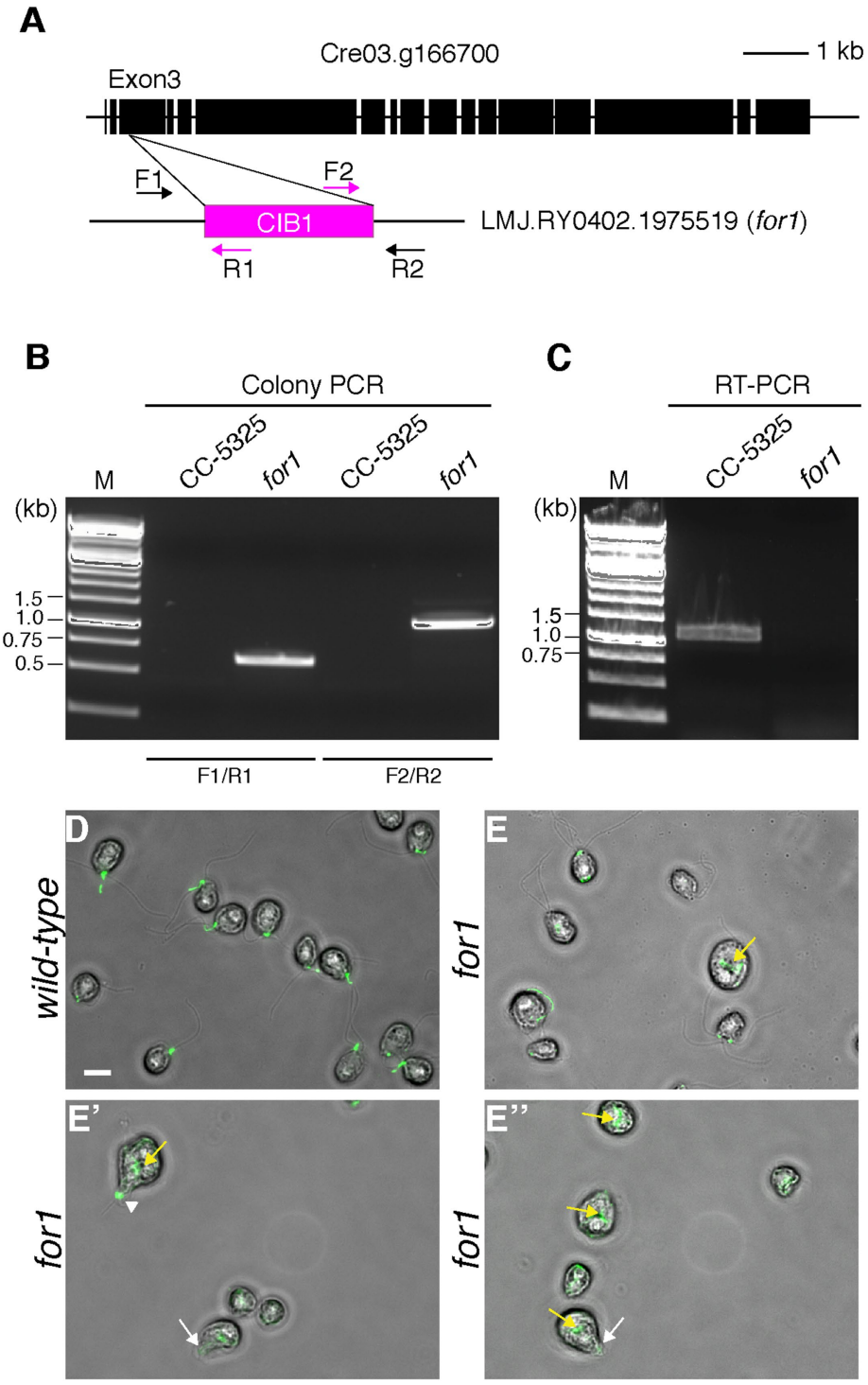

FIGURE 7: Insertional mutant of *FOR1* fails to make fertilization tubules. (A) Diagram of *Chlamydomonas FOR1* gene. Exons are shown as black rectangles. The CIB1 cassette is inserted in the exon3 of Cre03.g166700 in the *for1* mutant. Arrows indicate primer locations for detecting the cassette insertion. (B) Examination of the genome–cassette junctions by PCR from genomic DNA in the wild type parent strain (CC-5325) or the formin mutant (*for1*). (C) RT-PCR of the functional domain, FH2, of formin in wild-type (CC-5325) and the formin mutant (*for1*). (D–E") Alexa Fluor 488 phalloidin-labeled fertilization tubules in wild-type (D) and *for1* mutant (E–E") cells. Scale bar, 5 μm. The *for1* mutants retain midcell actin labeling (yellow arrows) and have apical protrusions where tubules should form (white arrows). A collection of labeled actin could sometimes be seen at the tip of the protrusion (white arrowhead).

Profilins have been shown to regulate both formin and Arp2/3 complex activity by differentially favoring access of actin monomers to formin over Arp2/3 complex (Rotty *et al.*, 2015; Suarez *et al.*, 2015; Suarez and Kovar, 2016). PRF1 may also be involved in regulating competition for actin by different assembly factors. *Chlamydomonas* contains ARP2 and ARP3, but its activators have not been identified (Kollmar *et al.*, 2012). The Arp2/3 complex may be involved in assembly and maintenance of the F-actin involved in flagellar membrane or protein trafficking, as treatment with Arp2/3 complex inhibitor CK-666 induces flagellar shortening (Avasthi *et al.*, 2014). The presence of multiple potential F-actin networks provides the possibility that other F-actin assembly factors are also present in *Chlamydomonas*. If so, PRF1 may be involved in regulating competition for actin monomers by these different assembly factors.

Furthermore, PRF1 also likely regulates both conventional actin IDA5 and NAP1 dynamics. Both SMIFH2 (unpublished data) and CK-666 (Avasthi *et al.*, 2014) affect flagellar length in mutants lacking conventional actin in which NAP1 is up-regulated. This finding suggests that both formin and Arp2/3 complex can nucleate NAP1 filaments. Unlike SMIFH2 and CK-666, latrunculin and cytochalasin do not affect NAP1. Loss of all F-actin networks by latrunculin treatment on a *nap1* mutant background caused delays in cytokinesis likely due to defects in chloroplast division (Onishi *et al.*, 2019). Future work will involve determining the nature of the F-actin networks involved in chloroplast division and flagellar protein trafficking as well as PRF1's role in ensuring proper F-actin distribution to each network.

FOR1 in fertilization tubule formation

FOR1 appears to be required for fertilization tubule formation as both *for1* mutants and wild-type gametes treated with the formin inhibitor SMIFH2 do not form fertilization tubules. We recently showed that while actin is up-regulated during fertilization tubule formation, increased actin expression is not required for tubule formation (Craig *et al.*, 2019). Because the failure to assemble tubules in *for1* mutants preserves the midcell actin population unlike cells that form tubules normally, FOR1-mediated filament assembly may compete for monomers in the existing pool required for maintaining the midcell F-actin network.

Fertilization tubule formation in *Chlamydomonas* occurs near the membrane at

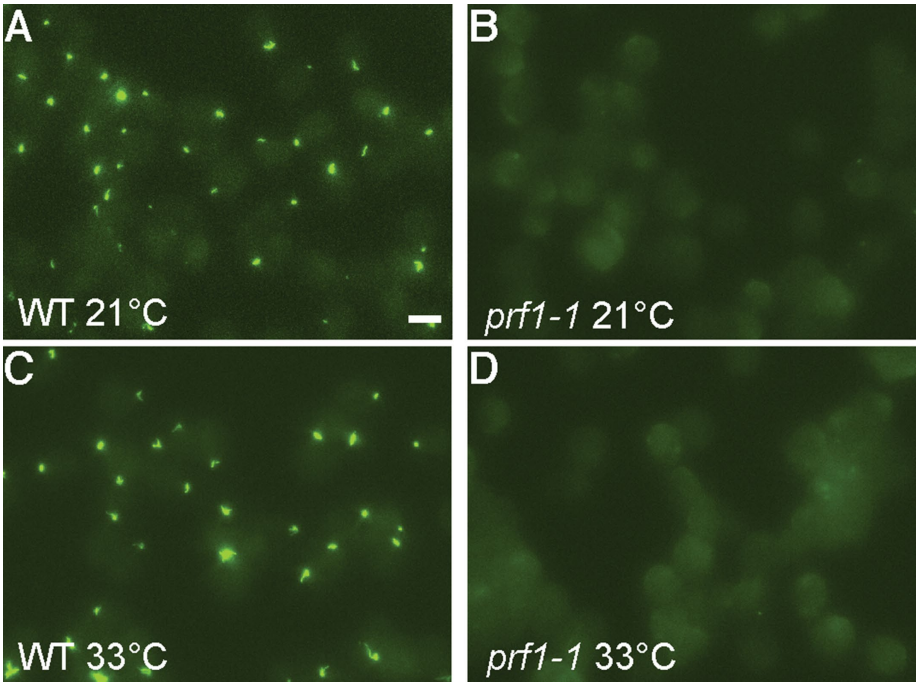

FIGURE 8: Profilin mutants fail to make fertilization tubules. (A–D) Wild-type and profilin mutant (*prf1-1*) cells stained with Alexa Fluor 488 phalloidin to label F-actin–rich fertilization tubules. (A) Wild-type cells at the permissive temperature, 21°C. Scale bar, 5 µm. (B) Temperature-sensitive *prf1-1* mutants at the permissive temperature, 21°C. (C) Wild-type cells at the restrictive temperature, 33°C. (D) Temperature-sensitive *prf1-1* mutants at the restrictive temperature, 33°C.

a site between the two flagella. Before fertilization tubule formation, this site is characterized by two parallel electron-dense regions called the membrane zone (immediately adjacent to the membrane) and doublet zone (slightly interior) (Goodenough and Weiss, 1975; Detmers *et al.*, 1983). In a mature fertilization tubule, the pointed ends of actin filaments are attached at the doublet zone (Detmers *et al.*, 1983), while the membrane zone is present at the far end of the extended fertilization tubule, near the F-actin barbed ends. As formins are frequently membrane-anchored, FOR1 is potentially localized to the membrane zone, which extends away from the doublet zone following F-actin formation. FOR1 could additionally be important for bundling the actin filaments in the fertilization tubule (Supplemental Figure S1), creating a stable projection.

Future work will involve determining the factors that regulate FOR1 activity and other ABPs that are involved in proper organization of F-actin at fertilization tubules and elsewhere.

MATERIALS AND METHODS

Plasmid construction

Constructs containing different components of the formin actin assembly domains (FH1 and FH2) were prepared for bacterial expression. The preparation of Cdc12(FH1FH2) and Cdc12(FH1) constructs has been described (Neidt *et al.*, 2009). The FOR1 domain constructs were designed based on sequence analysis of the *Chlamydomonas* genome and Expressed Sequence Tag analysis by Susan Dutcher (Washington University, St. Louis, MO) and were optimized for bacterial expression and custom synthesized (DNA 2.0, Newark, CA). Constructs were designed by SnapGene software (from GSL Biotech; available at snapgene.com). All constructs were prepared by standard cloning procedures, consisting of PCR amplification (iProof, Bio-Rad Laboratories) from the commercially prepared DNA. Restriction enzyme cleavage sites and 6× His sequences were included in the reverse primers. PCR products were cloned using restriction enzymes into pET21a (EMD Biosciences) for expression. All amplified sequences were confirmed by sequencing.

Protein purification

All constructs of FOR1 and PRF1 were expressed in BL21-Codon Plus (DE3)-RP (Agilent Technologies, Santa Clara, CA). Cdc12(FH1FH2) (Kovar and Pollard, 2004), SpPRF (Lu and Pollard, 2001), SpFus1 (Scott *et al.*, 2011), and PRF1 (Kovar *et al.*, 2001) were purified as described previously. FOR1 constructs were His-tag affinity purified. FOR1 constructs were expressed with 0.5 mM isopropyl ß-D-thiogalactopyranoside (IPTG; Sigma-Aldrich) for 16 h at 16°C. Cells were resuspended in extraction buffer (50 mM NaH_2PO_4, pH 8.0, 500 mM NaCl, 10% glycerol, 10 mM imidazole, 10 mM betamercaptoethanol [ßME]) supplemented with 0.5 mM phenylmethylsulfonyl fluoride and protease inhibitors, sonicated, and homogenized in an Emulsiflex-C3 (Avestin, Ottawa, ON, Canada). The homogenate was spun and clarified at 30,000 × *g* for 15 min, then 50,000 × *g* for 30 min, and incubated with Talon Metal Affinity Resin (Clontech, Mountain View, CA) for 1 h at 4°C. The resin was loaded onto a disposable column and washed with 50 ml wash with extraction buffer. FOR1 was then eluted with Talon elution buffer (50 mM NaH_2PO_4, pH 8.0, 500 mM NaCl, 10% glycerol, 250 mM imidazole, 10 mM ßME) and dialyzed into formin buffer (20 mM HEPES, pH 7.4, 1 mM EDTA, 200 mM KCl, 0.01% NaN_3, and 1 mM dithiothreitol [DTT]).

A_{280} of purified proteins was taken using a Nanodrop 2000c Spectrophotometer (Thermo-Scientific, Waltham, MA). Protein concentrations were determined based on extinction coefficients estimated from amino acid sequences using ProtParam (http://web.expasy.org/protparam/), or from previous studies: PRF1: 19,190 M^{-1} (Kovar *et al.*, 2001), SpPRF: 20,065 M^{-1} (Lu and Pollard, 2001), FOR1(10P,FH2): 29,450 M^{-1}, FOR1(3P,FH2): 24,200 M^{-1}, FOR1(FH2): 24,400 M^{-1}, SNAP-FOR1(3P,FH2): 44,920 M^{-1}, and Cdc12 (FH1,FH2): 51,255 M^{-1} (Kovar *et al.*, 2003). Protein concentrations of FH1 constructs Cdc12(FH1), FOR1(FH1), and FOR1(3P) were determined by A_{205} in water ([(A_{205}FH1–A_{205}buffer)/30]/mol wt). Proteins were flash-frozen in liquid nitrogen and kept at –80°C. SNAP-FOR1(3P,FH2) protein was labeled with SNAP-549 dye (New England Biolabs, Ipswich, MA) as per manufacturer's instructions before each TIRF experiment.

Actin was purified from rabbit or chicken skeletal muscle actin as previously described (Spudich and Watt, 1971). For pyrene assembly assays, actin was labeled with *N*-(1-pyrene)Iodoacetamide (Life Technologies, Carlsbad, CA) on Cys-374. As the combination of FOR1 in the presence of PRF1 selected against actin labeled on Cys-374, actin labeled with Alexa Fluor 488 on lysines (ThermoFisher Scientific, Waltham, MA) was used for TIRF microscopy experiments.

Pyrene assembly and disassembly assays

All pyrene assembly and disassembly assays were carried out in a 96-well plate, and the fluorescence of pyrene-actin (excitation at

364 nm and emission at 407 nm) was measured with a Spectramax Gemini XPS (Molecular Devices) or Safire2 (Tecan) fluorescence plate reader as described (Zimmermann *et al.*, 2016). For spontaneous assembly assays, a 15-µM mixture of 20% pyrene-labeled Mg-ATP-actin monomer with 100× anti-foam 204 (0.005%; Sigma) was placed in the upper well of a 96 well nonbinding black plate. Formin and/or profilin, 10X KMEI (500 mM KCl, 10 mM $MgCl_2$, 10 mM ethylene glycol tetraacetic acid [EGTA], and 100 mM imidazole, pH 7.0) and Mg-Buffer G (2 mM Tris, pH 8.0, 0.2 mM ATP, 0.1 mM $MgCl_2$, and 0.5 mM DTT) were placed in the lower row of the plate. Reactions were initiated by mixing contents of the lower wells the actin monomers in the upper wells with a 12-channel pipetman (Eppendorf). For pyrene assembly assays involving SMIFH2, SMIFH2 was added to the lower wells containing FOR1 prior to mixing the upper and lower wells.

For seeded assembly assays, 5.0 µM of unlabeled Mg-ATP-actin was preassembled in the upper row of the plate, followed by the addition of anti-foam, formin and/or profilin, and Mg-Buffer G. A 2.0-µM mixture of 20% pyrene-labeled actin with Mg-Buffer G was placed in the lower plate row. Mixing actin monomers in lower wells with preassembled actin filaments in upper wells initiated reactions.

For depolymerization assays, a 5.0-µM mixture of unlabeled and 50% pyrene-labeled Mg-ATP-actin monomers was preassembled in the upper row of the plate for 2 h, followed by the addition of anti-foam. Formin, 10× KMEI, and Mg-Buffer G were placed in the lower plate row. Reactions were initiated by mixing lower wells with upper wells, diluting the preassembled filaments to 0.1 µM.

Profilin FH1 affinity assays

The affinity of profilin for formin(FH1) was determined by measuring the change in profilin's intrinsic tryptophan fluorescence by excitation at 295 nm and emission at 323 nm (Perelroizen *et al.*, 1994; Petrella *et al.*, 1996). Profilin (1.0 µM) was incubated with a range of poly-L-proline or formin(FH1) concentrations for 30 min, and then profilin fluorescence was read in a Safire2 fluorescence plate reader and plotted versus formin(FH1) concentration. The fluorescence of formin(FH1) alone was subtracted from the fluorescence in the presence of profilin. Dissociation constants (K_d) were determined by fitting a quadratic function to the dependence of the concentration of bound profilin on the concentration of formin(FH1).

Polymerization and depolymerization rate determination

Actin assembly rates were determined from spontaneous assembly reactions by measuring the slopes of actin assembly following the lag phase to 50% of total actin assembly. Assembly rates from preassembled actin seeds were determined by a linear fit to the first 100 s of assembly. Depolymerization rates were determined by a linear fit to the first 100–300 s of the reaction.

The affinity of FOR1 for barbed ends was determined as previously described (Kovar *et al.*, 2003). We fitted the plot of the dependence of the assembly or disassembly rate on formin concentration using the equation $V_i = V_{if} + (V_{ib} - V_{if})\ ((K_d + [\text{ends}] + [\text{formin}] - \sqrt{((K_d + [\text{ends}] + [\text{formin}])2 - 4[\text{ends}][\text{formin}])/2[\text{ends}])}$, where V_i is the observed elongation or depolymerization rate, V_{if} is the elongation or depolymerization rate of free barbed ends, V_{ib} is the elongation or depolymerization rate of bound barbed ends, [ends] are the concentration of barbed ends, and [formin] is formin concentration. The nucleation efficiency was calculated by dividing the slope of the spontaneous assembly rate by *k+* in the absence and presence of profilin and dividing by the formin concentration (Kovar *et al.*, 2006). Depolymerization rates are normalized to the rate of actin assembly alone and expressed as a percentage of the standard actin assembly rate.

Fluorescence micrographs (rhodamine phalloidin)

Unlabeled Mg-ATP-actin was assembled as per standard spontaneous assembly reactions. Actin filaments were then incubated with 1 µM TRITC-Phalloidin (Fluka Biochemika, Switzerland) for 5 min. Reactions were terminated by diluting assembled filaments in fluorescence buffer (50 mM KCl, 1 mM $MgCl_2$, 100 mM DTT, 20 µg/ml catalase, 100 µg/ml glucose oxidase, 3 mg/ml glucose, 0.5% methylcellulose, and 10 mM imidazole, pH 7.0) and were absorbed to coverslips coated with 0.05 µg/µl poly-L-lysine. Fluorescence microscopy images were collected on an Olympus IX-81 microscope and cooled CCD camera (Orca-ER, Hamamatsu).

Low-speed sedimentation assays

Sedimentation assays were performed as previously described (Zimmermann *et al.*, 2016). Mg-ATP actin (15 µM) monomers were spontaneously assembled for 1 h in 10 mM imidazole, pH 7.0, 50 mM KCl, 5 mM $MgCl_2$, 1 mM EGTA, 0.5 mM DTT, 0.2 mM ATP, and 90 µM $CaCl_2$ to generate F-actin. F-actin was then incubated with FOR1 or SpFus1 for 20 min at 25°C and spun at 10,000 × *g* at 25°C. Supernatant and pellets were separated by 15% SDS–PAGE gel electrophoresis and stained with Coomassie Blue for 30 min, destained for 16 h, and analyzed by densitometry with ImageJ (Schneider *et al.*, 2012; http://imagej.net).

TIRF microscopy

Time-lapse TIRF microscopy movies were obtained using a iXon EMCCD camera (Andor Technology, Belfast, UK) fitted to an Olympus IX-71 microscope with through-the-objective TIRF illumination as described (Zimmermann *et al.*, 2016). Mg-ATP-actin (10–20% Alexa-488 labeled) was mixed with a polymerization mix (10 mM imidazole [pH 7.0], 50 mM KCl, 1 mM $MgCl_2$, 1 mM EGTA, 50 mM DTT, 0.2 mM ATP, 50 µM $CaCl_2$, 15 mM glucose, 20 µg/ml catalase, 100 µg/ml glucose oxidase, and 0.5% [400 cP] methylcellulose) to induce F-actin assembly (Winkelman *et al.*, 2014). Where stated, formin or profilin was added to the polymerization mix prior to mixing with actin and initiating F-actin polymerization. The mixture was then added to a flow chamber and imaged at 10-s intervals at room temperature. For bead assays, Wsp1 and formin beads were prepared as previously described (Loisel *et al.*, 1999). Carboxylated Polybeads (Polysciences, Warrington, PA) were coated with Wsp1 or unlabeled SNAP-FOR1(3P,FH2) and flowed into the TIRF chamber prior to initiating the reaction.

Fertilization tubule assay

Wild-type 137c (CC-125 mt+) *C. reinhardtii* cells were obtained from the *Chlamydomonas* Resource Center (University of Minnesota). To induce gametogenesis, cells were grown in M-N (M1 minimal media without nitrogen) overnight under growth lighting. Gametes were mixed with dibutyryl cAMP (13.5 mM) and papaverine (135 µM) to induce fertilization tubule formation along with different inhibitor preparations; untreated, 1% DMSO (solvent for all inhibitors), 10 µM LatB, 10 µM SMIFH2, 100 µM SMIFH2, and 100 µM CK-666. Cells were placed on a rotator under a LumiBar LED light source (LumiGrow) for 2 h. After fertilization tubule induction, cells were adhered to coverslips coated with poly-lysine and fixed with 4% paraformaldehyde in 10 mM HEPES. They were permeabilized with –20°C acetone, stained with 100 nM Alexa Fluor 488 phalloidin (Life Technologies) according to manufacturer protocols and mounted on slides with Fluoromount-G (Southern Biotech) for imaging. Slides were imaged with a Nikon Ti-S widefield fluorescence microscope using a Plan Achromat 100×/1.25 NA oil immersion objective lens, a QICam fast 1394 CCD digital camera (QImaging), and NIS Elements software.

All cells in multiple fields of view (~50–100 cells per condition) were counted for the presence of fertilization tubules using the ImageJ Cell Counter plugin to determine tubule percentage (#tubules/# total cells) × 100. Means and standard deviations are plotted for experiments done in triplicate. Results were analyzed with one-way analysis of variance and Dunnett's multiple comparison post hoc test. For fertilization tubule measurements, line segments were drawn onto projected FITC images and fitted with splines using ImageJ; $n > 45$ measurements were collected following a pixel to micron ratio conversion for the optical setup and compared using Kruskal–Wallis and Dunn's multiple comparison tests.

Colony PCR, RNA extraction, and RT-PCR

Colony PCR was performed as previously described (Cao *et al*., 2009). The genome–cassette junctions were amplified via PCR by using different primers set. The primers set F1/R1 or F2/R2 is used to amplify the left or right insert junction, respectively (F1: ATCAGGAGCCCCCTGTATTT; R1: GCACCAATCATGTCAAGCCT; F2: GACGTTACAGCACACCCTTG; R2: CACCTGACGTGTTGTTGACC). Total RNA was isolated with PureLink RNA Mini Kit (Thermo Fisher Scientific). To avoid genomic DNA contamination, on-column PureLink DNase (Thermo Fisher Scientific) treatment was performed. First-strand cDNA was synthesized from 1 g purified total RNA with SuperScript III First-Strand Synthesis system (Thermo Fisher Scientific). For reverse transcription PCR (RT-PCR), cDNA fragment coding the majority of the formin FH2 domain was amplified using gene-specific primers For1_F and For1_R (For1_F: CTCCCCCTCCGGTTATGAG; For1_R: CAGACAGCTCGTTCAGCTTG). For both colony PCR and RT-PCR, Phusion High-Fidelity DNA Polymerase (New England Biolabs) was used, and the amplification conditions were as follows: 98°C for 30 s, followed by 35 cycles of 98°C for 10 s, 65°C for 10 s, and 72°C for 60 s.

ACKNOWLEDGMENTS

We thank Susan Dutcher (Washington University in St. Louis) and Bill Snell (UT Southwestern) for helpful discussions, including confirmation that *Chlamydomonas* expresses FOR1. We thank Megan Rhyne (University of Tennessee, Knoxville) for helpful comments. This work was supported by National Institutes of Health grants R01 GM079265 (to D.R.K.) and P20 GM104936 (to P.A.), National Institutes of Health Molecular and Cellular Biology Training Grant T32 GM007183 (to J.R.C.), and National Institutes of Health Medical Scientist Training Program Training Grant T32 GM007281 (to M.J.G.).

REFERENCES

Avasthi P, Onishi M, Karpiak J, Yamamoto R, Mackinder L, Jonikas MC, Sale WS, Shoichet B, Pringle JR, Marshall WF (2014). Actin is required for IFT regulation in Chlamydomonas reinhardtii. Curr Biol 24, 2025–2032.

Bestul AJ, Christensen JR, Grzegorzewska AP, Burke TA, Sees JA, Carroll RT, Sirotkin V, Keenan RJ, Kovar DR (2015). Fission yeast profilin is tailored to facilitate actin assembly by the cytokinesis formin Cdc12. Mol Biol Cell 26, 283–293.

Breitsprecher D, Goode BL (2013). Formins at a glance. J Cell Sci 126, 1–7.

Cao M, Fu Y, Guo Y, Pan J (2009). Chlamydomonas (Chlorophyceae) colony PCR. Protoplasma 235, 107–110.

Carlsson L, Nystrom LE, Sundkvist I, Markey F, Lindberg U (1977). Actin polymerizability is influenced by profilin, a low molecular weight protein in non-muscle cells. J Mol Biol 115, 465–483.

Courtemanche N, Pollard TD. (2013). Interaction of profilin with the barbed end of actin filaments. Biochemistry 52, 6456–6466.

Craig EW, Avasthi P (2019). Visualizing filamentous actin in *Chlamydomonas reinhardtii*. Bio-Protocol 9, e3274.

Craig EW, Mueller DM, Bigge BM, Schaffer M, Engel BD, Avasthi P (2019). The elusive actin cytoskeleton of a green alga expressing both conventional and divergent actins. Mol Biol Cell 30, 2827–2837.

Detmers PA, Carboni JM, Condeelis J (1985). Localization of actin in Chlamydomonas using antiactin and NBD-phallacidin. Cell Motil 5, 415–430.

Detmers PA, Goodenough UW, Condeelis J (1983). Elongation of the fertilization tubule in Chlamydomonas: new observations on the core microfilaments and the effect of transient intracellular signals on their structural integrity. J Cell Biol 97, 522–532.

Goldschmidt-Clermont PJ, Kim JW, Machesky LM, Rhee SG, Pollard TD (1991). Regulation of phospholipase C-gamma 1 by profilin and tyrosine phosphorylation. Science 251, 1231–1233.

Goodenough UW, Weiss RL (1975). Gametic differentiation in Chlamydomonas reinhardtii. III. Cell wall lysis and microfilament-associated mating structure activation in wild-type and mutant strains. J Cell Biol 67, 623–637.

Gould CJ, Maiti S, Michelot A, Graziano BR, Blanchoin L, Goode BL (2011). The formin DAD domain plays dual roles in autoinhibition and actin nucleation. Curr Biol 21, 384–390.

Gutsche-Perelroizen I, Lepault J, Ott A, Carlier M-F (1999). Filament assembly from profilin-actin. J Biol Chem 274, 6234–6243.

Hansen SD, Mullins RD (2010). VASP is a processive actin polymerase that requires monomeric actin for barbed end association. J Cell Biol 191, 571–584.

Harper JD, McCurdy DW, Sanders MA, Salisbury JL, John PC (1992). Actin dynamics during the cell cycle in Chlamydomonas reinhardtii. Cell Motil Cytoskeleton 22, 117–126.

Hirono M, Uryu S, Ohara A, Kato-Minoura T, Kamiya R (2003). Expression of conventional and unconventional actins in Chlamydomonas reinhardtii upon deflagellation and sexual adhesion. Eukaryot Cell 2, 486–493.

Isogai T, van der Kammen R, Innocenti M (2015). SMIFH2 has effects on formins and p53 that perturb the cytoskeleton. Sci Rep 5, 9802.

Jack B, Mueller DM, Fee AC, Tetlow AL, Avasthi P (2019). Partially redundant actin genes in Chlamydomonas control transition zone organization and flagellum-directed traffic. Cell Rep 27, 2459–2467.

Kaiser DA, Vinson VK, Murphy DB, Pollard TD (1999). Profilin is predominantly associated with monomeric actin in Acanthamoeba. J Cell Sci 112, 3779–3790.

Kato-Minoura T, Hirono M, Kamiya R (1997). Chlamydomonas inner-arm dynein mutant, ida5, has a mutation in an actin-encoding gene. J Cell Biol 137, 649–656.

Kato-Minoura T, Uryu S, Hirono M, Kamiya R (1998). Highly divergent actin expressed in a Chlamydomonas mutant lacking the conventional actin gene. Biochem Biophys Res Commun 251, 71–76.

Kinosian HJ, Selden LA, Gershman LC, Estes JE (2002). Actin filament barbed-end elongation with nonmuscle MgATP-actin and MgADP-actin in the presence of profilin. Biochemistry 41, 6734–6743.

Kollmar M, Lbik D, Enge S (2012). Evolution of the eukaryotic ARP2/3 activators of the WASP family: WASP, WAVE, WASH, and WHAMM, and the proposed new family members WAWH and WAML. BMC Res Notes 5, 88.

Kovar DR (2006). Molecular details of formin-mediated actin assembly. Curr Opin Cell Biol 18, 11–17.

Kovar DR, Harris ES, Mahaffy R, Higgs HN, Pollard TD (2006). Control of the assembly of ATP- and ADP-actin by formins and profilin. Cell 124, 423–435.

Kovar DR, Kuhn JR, Tichy AL, Pollard TD (2003). The fission yeast cytokinesis formin Cdc12p is a barbed end actin filament capping protein gated by profilin. J Cell Biol 161, 875–887.

Kovar DR, Pollard TD (2004). Insertional assembly of actin filament barbed ends in association with formins produces piconewton forces. Proc Natl Acad Sci USA 101, 14725–14730.

Kovar DR, Yang P, Sale WS, Drobak BK, Staiger CJ (2001). Chlamydomonas reinhardtii produces a profilin with unusual biochemical properties. J Cell Sci 114, 4293–4305.

Lee VD, Finstad SL, Huang B (1997). Cloning and characterization of a gene encoding an actin-related protein in Chlamydomonas. Gene 197, 153–159.

Loisel TP, Boujemaa R, Pantaloni D, Carlier MF (1999). Reconstitution of actin-based motility of Listeria and Shigella using pure proteins. Nature 401, 613–616.

Lu J, Pollard TD (2001). Profilin binding to poly-L-proline and actin monomers along with ability to catalyze actin nucleotide exchange is required for viability of fission yeast. Mol Biol Cell 12, 1161–1175.

Merchant SS, Prochnik SE, Vallon O, Harris EH, Karpowicz SJ, Witman GB, Terry A, Salamov A, Fritz-Laylin LK, Maréchal-Drouard L, *et al*. (2007). The Chlamydomonas genome reveals the evolution of key animal and plant functions. Science 318, 245–250.

Mockrin SC, Korn ED (1980). Acanthamoeba profilin interacts with G-actin to increase the rate of exchange of actin-bound adenosine 5′-triphosphate. Biochemistry 19, 5359–5362.
Neidt EM, Scott BJ, Kovar DR (2009). Formin differentially utilizes profilin isoforms to rapidly assemble actin filaments. J Biol Chem 284, 673–684.
Nolen BJ, Tomasevic N, Russell A, Pierce DW, Jia Z, McCormick CD, Hartman J, Sakowicz R, Pollard TD (2009). Characterization of two classes of small molecule inhibitors of Arp2/3 complex. Nature 460, 1031–1035.
Onishi M, Pecani K, Jones T, Pringle JR, Cross FR (2018). F-actin homeostasis through transcriptional regulation and proteasome-mediated proteolysis. Proc Natl Acad Sci USA 115, E6487–E6496.
Onishi M, Pringle JR, Cross FR (2016). Evidence that an unconventional actin can provide essential F-actin function and that a surveillance system monitors F-actin integrity in Chlamydomonas. Genetics 202, 977–996.
Onishi M, Umen JG, Cross FR, Pringle JR (2019). Cleavage-furrow formation without F-actin in Chlamydomonas. biorXiv, doi.org/10.1101/789016.
Otomo T, Tomchick DR, Otomo C, Panchal SC, Machius M, Rosen MK (2005). Structural basis of actin filament nucleation and processive capping by a formin homology 2 domain. Nature 433, 488–494.
Perelroizen I, Didry D, Christensen H, Chua NH, Carlier MF (1996). Role of nucleotide exchange and hydrolysis in the function of profilin in action assembly. J Biol Chem 271, 12302–12309.
Perelroizen I, Marchand JB, Blanchoin L, Didry D, Carlier MF (1994). Interaction of profilin with G-actin and poly(L-proline). Biochemistry 33, 8472–8478.
Pernier J, Shekhar S, Jegou A, Guichard B, Carlier M-F (2016). Profilin interaction with actin filament barbed end controls dynamic instability, capping, branching, and motility. Dev Cell 36, 201–214.
Petrella EC, Machesky LM, Kaiser DA, Pollard TD (1996). Structural requirements and thermodynamics of the interaction of proline peptides with profilin. Biochemistry 35, 16535–16543.
Pollard TD, Cooper JA (1984). Quantitative analysis of the effect of Acanthamoeba profilin on actin filament nucleation and elongation. Biochemistry 23, 6631–6641.
Rizvi SA, Neidt EM, Cui J, Feiger Z, Skau CT, Gardel ML, Kozmin SA, Kovar DR (2009). Identification and characterization of a small molecule inhibitor of formin-mediated actin assembly. Chem Biol 16, 1158–1168.
Rotty JD, Wu C, Haynes EM, Suarez C, Winkelman JD, Johnson HE, Haugh JM, Kovar DR, Bear JE (2015). Profilin-1 serves as a gatekeeper for actin assembly by Arp2/3-dependent and -independent pathways. Dev Cell 32, 54–67.
Schneider CA, Rasband WS, Eliceiri KW (2012). NIH Image to ImageJ: 25 years of image analysis. Nat Methods 9, 671–675.
Schutt CE, Myslik JC, Rozycki MD, Goonesekere NC, Lindberg U (1993). The structure of crystalline profilin-beta-actin. Nature 365, 810–816.
Scott BJ, Neidt EM, Kovar DR (2011). The functionally distinct fission yeast formins have specific actin-assembly properties. Mol Biol Cell 22, 3826–3839.
Spudich JA, Watt S (1971). The regulation of rabbit skeletal muscle contraction. I. Biochemical studies of the interaction of the tropomyosin-troponin complex with actin and the proteolytic fragments of myosin. J Biol Chem 246, 4866–4871.
Suarez C, Carroll RT, Burke TA, Christensen JR, Bestul AJ, Sees JA, James ML, Sirotkin V, Kovar DR (2015). Profilin regulates F-actin network homeostasis by favoring formin over Arp2/3 complex. Dev Cell 32, 43–53.
Suarez C, Kovar DR (2016). Internetwork competition for monomers governs actin cytoskeleton organization. Nat Rev Mol Cell Biol 17, 799–810.
Tulin F, Cross FR (2014). A microbial avenue to cell cycle control in the plant superkingdom. Plant Cell 26, 4019–4038.
Wilson NF, Foglesong MJ, Snell WJ (1997). The Chlamydomonas mating type plus fertilization tubule, a prototypic cell fusion organelle: isolation, characterization, and in vitro adhesion to mating type minus gametes. J Cell Biol 137, 1537–1553.
Winkelman JD, Bilancia CG, Peifer M, Kovar DR (2014). Ena/VASP Enabled is a highly processive actin polymerase tailored to self-assemble parallel-bundled F-actin networks with Fascin. Proc Natl Acad Sci USA 111, 4121–4126.
Zimmermann D, Morganthaler AN, Kovar DR, Suarez C (2016). In vitro biochemical characterization of cytokinesis actin-binding proteins. Methods Mol Biol 1369, 151–179.